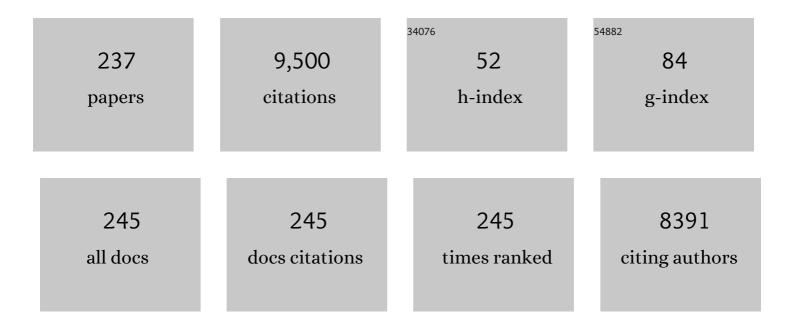
Julie Cairney

List of Publications by Year in descending order

Source: https://exaly.com/author-pdf/9366577/publications.pdf Version: 2024-02-01



#	Article	IF	CITATIONS
1	Cu2ZnSnS4 solar cells with over 10% power conversion efficiency enabled by heterojunction heat treatment. Nature Energy, 2018, 3, 764-772.	19.8	623
2	Atom Probe Microscopy. Springer Series in Materials Science, 2012, , .	0.4	501
3	Observation of hydrogen trapping at dislocations, grain boundaries, and precipitates. Science, 2020, 367, 171-175.	6.0	275
4	Microstructural evolution during ageing of Al–Cu–Li–x alloys. Acta Materialia, 2014, 66, 199-208.	3.8	183
5	Long-Chain Terminal Alcohols through Catalytic CO Hydrogenation. Journal of the American Chemical Society, 2013, 135, 7114-7117.	6.6	169
6	Dynamic precipitation, segregation and strengthening of an Al-Zn-Mg-Cu alloy (AA7075) processed by high-pressure torsion. Acta Materialia, 2019, 162, 19-32.	3.8	166
7	Atom probe crystallography. Materials Today, 2012, 15, 378-386.	8.3	158
8	New insights into the phase transformations to isothermal ω and ω-assisted α in near β-Ti alloys. Acta Materialia, 2016, 106, 353-366.	3.8	155
9	Characterizing deformed ultrafine-grained and nanocrystalline materials using transmission Kikuchi diffraction in a scanning electron microscope. Acta Materialia, 2014, 62, 69-80.	3.8	142
10	Transmission Kikuchi diffraction in a scanning electron microscope: A review. Materials Science and Engineering Reports, 2016, 110, 1-12.	14.8	138
11	Deformation-induced trace element redistribution in zircon revealed using atom probe tomography. Nature Communications, 2016, 7, 10490.	5.8	137
12	A reproducible method for damageâ€free siteâ€specific preparation of atom probe tips from interfaces. Microscopy Research and Technique, 2012, 75, 484-491.	1.2	134
13	Atom probe tomography. Nature Reviews Methods Primers, 2021, 1, .	11.8	131
14	Effect of ion irradiation on tensile ductility, strength and fictive temperature in metallic glass nanowires. Acta Materialia, 2014, 74, 165-182.	3.8	130
15	Observations of grain boundary impurities in nanocrystalline Al and their influence on microstructural stability and mechanical behaviour. Acta Materialia, 2012, 60, 1038-1047.	3.8	122
16	Phase Stability of <i>t</i> ′â€Zirconiaâ€Based Thermal Barrier Coatings: Mechanistic Insights. Journal of the American Ceramic Society, 2011, 94, s168.	1.9	119
17	Isolated copper–tin atomic interfaces tuning electrocatalytic CO2 conversion. Nature Communications, 2021, 12, 1449.	5.8	119

Nanocomposite Tiâ€"Siâ€"N, Zrâ€"Siâ€"N, Tiâ€"Alâ€"Siâ€"N, Tiâ€"Alâ€"Vâ€"Siâ€"N thin film coatings deposited by yacuum arc deposition. Surface and Coatings Technology, 2005, 200, 2228-2235.

Julie Cairney

#	Article	IF	CITATIONS
19	Penetration of protective chromia scales by carbon. Scripta Materialia, 2014, 77, 29-32.	2.6	113
20	Cd-Free Cu ₂ ZnSnS ₄ solar cell with an efficiency greater than 10% enabled by Al ₂ O ₃ passivation layers. Energy and Environmental Science, 2019, 12, 2751-2764.	15.6	112
21	Atomic-scale compositional mapping reveals Mg-rich amorphous calcium phosphate in human dental enamel. Science Advances, 2016, 2, e1601145.	4.7	107
22	On the multiplicity of field evaporation events in atom probe: A new dimension to the analysis of mass spectra. Philosophical Magazine Letters, 2010, 90, 121-129.	0.5	96
23	Strengthening from Nb-rich clusters in a Nb-microalloyed steel. Scripta Materialia, 2012, 66, 710-713.	2.6	91
24	The effect of coordination environment on the activity and selectivity of single-atom catalysts. Coordination Chemistry Reviews, 2022, 461, 214493.	9.5	91
25	Increasing the strength of nanocrystalline steels by annealing: Is segregation necessary?. Scripta Materialia, 2015, 95, 27-30.	2.6	89
26	Reducing the macroparticle content of cathodic arc evaporated TiN coatings. Surface and Coatings Technology, 2004, 183, 283-294.	2.2	87
27	Fatigue properties of AlSi10Mg produced by Additive Layer Manufacturing. International Journal of Fatigue, 2019, 119, 160-172.	2.8	86
28	Tunable Syngas Production through CO ₂ Electroreduction on Cobalt–Carbon Composite Electrocatalyst. ACS Applied Materials & Interfaces, 2020, 12, 9307-9315.	4.0	79
29	The mechanism of ω-assisted α phase formation in near β-Ti alloys. Scripta Materialia, 2015, 104, 75-78.	2.6	75
30	Dynamic reconstruction for atom probe tomography. Ultramicroscopy, 2011, 111, 1619-1624.	0.8	72
31	Superelasticity and Tunable Thermal Expansion across a Wide Temperature Range. Journal of Materials Science and Technology, 2016, 32, 705-709.	5.6	72
32	Atom probe specimen fabrication methods using a dual FIB/SEM. Ultramicroscopy, 2007, 107, 756-760.	0.8	71
33	Understanding solid solution strengthening at elevated temperatures in a creep-resistant Mg–Gd–Ca alloy. Acta Materialia, 2019, 181, 185-199.	3.8	71
34	Three-dimensional investigation of particle-stimulated nucleation in a nickel alloy. Acta Materialia, 2007, 55, 5157-5167.	3.8	68
35	Designing Undercoordinated Ni–N _{<i>x</i>} and Fe–N _{<i>x</i>} on Holey Graphene for Electrochemical CO ₂ Conversion to Syngas. ACS Nano, 2021, 15, 12006-12018.	7.3	68
36	Techniques for generating 3-D EBSD microstructures by FIB tomography. Materials Characterization, 2007, 58, 961-967.	1.9	66

#	Article	IF	CITATIONS
37	Degradation of TiN coatings under cyclic loading. Acta Materialia, 2004, 52, 3229-3237.	3.8	65
38	Synthesis and performance evaluation of thin film PPy-PVDF multilayer electroactive polymer actuators. Sensors and Actuators A: Physical, 2011, 165, 321-328.	2.0	65
39	Atomic-Level Insights into the Edge Active ReS ₂ Ultrathin Nanosheets for High-Efficiency Light-to-Hydrogen Conversion. , 2020, 2, 1484-1494.		65
40	Phase Evolution upon Aging of Air Plasma Sprayed tâ€2â€Zirconia Coatings: <scp>II</scp> –Microstructure Evolution. Journal of the American Ceramic Society, 2013, 96, 299-307.	1.9	63
41	Precipitation and clustering in the early stages of ageing in Inconel 718. Materials Science & Engineering A: Structural Materials: Properties, Microstructure and Processing, 2010, 527, 7770-7774.	2.6	61
42	Investigating the microstructure and composition of cold gas-dynamic spray (CGDS) Ti powder deposited on Al 6063 substrate. Surface and Coatings Technology, 2010, 204, 3739-3749.	2.2	61
43	Optimization of pulsed laser atom probe (PLAP) for the analysis of nanocomposite Ti–Si–N films. Ultramicroscopy, 2010, 110, 836-843.	0.8	60
44	Crystallographic structural analysis in atom probe microscopy via 3D Hough transformation. Ultramicroscopy, 2011, 111, 458-463.	0.8	59
45	Deformation mechanisms operating during nanoindentation of TiN coatings on steel substrates. Surface and Coatings Technology, 2005, 192, 11-18.	2.2	57
46	Elemental partitioning of platinum group metal containing Ni-base superalloys using electron microprobe analysis and atom probe tomography. Acta Materialia, 2010, 58, 1952-1962.	3.8	57
47	Atom probe crystallography: Atomic-scale 3-D orientation mapping. Scripta Materialia, 2012, 66, 907-910.	2.6	57
48	High Efficiency Cu ₂ ZnSn(S,Se) ₄ Solar Cells with Shallow Li _{Zn} Acceptor Defects Enabled by Solutionâ€Based Li Postâ€Deposition Treatment. Advanced Energy Materials, 2021, 11, 2003783.	10.2	57
49	The evolution of microstructure and mechanical properties of Ti–5Al–5Mo–5V–2Cr–1Fe during ageing. Journal of Alloys and Compounds, 2015, 629, 260-273.	2.8	56
50	New approaches to nanoparticle sample fabrication for atom probe tomography. Ultramicroscopy, 2015, 159, 413-419.	0.8	56
51	Enhanced photoelectrochemical water-splitting performance with a hierarchical heterostructure: Co3O4 nanodots anchored TiO2@P-C3N4 core-shell nanorod arrays. Chemical Engineering Journal, 2021, 404, 126458.	6.6	56
52	Segregation of B, P, and C in the Ni-Based Superalloy, Inconel 718. Metallurgical and Materials Transactions A: Physical Metallurgy and Materials Science, 2012, 43, 2183-2191.	1.1	54
53	An automated method of quantifying ferrite microstructures using electron backscatter diffraction (EBSD) data. Ultramicroscopy, 2014, 137, 40-47.	0.8	54
54	A quantitative atom probe study of the Nb excess at prior austenite grain boundaries in a Nb microalloyed strip-cast steel. Acta Materialia, 2012, 60, 5049-5055.	3.8	52

#	Article	lF	CITATIONS
55	Atom probe crystallography: Characterization of grain boundary orientation relationships in nanocrystalline aluminium. Ultramicroscopy, 2011, 111, 493-499.	0.8	51
56	FeS2 bridging function to enhance charge transfer between MoS2 and g–C3N4 for efficient hydrogen evolution reaction. Chemical Engineering Journal, 2021, 421, 127804.	6.6	51
57	Mining information from atom probe data. Ultramicroscopy, 2015, 159, 324-337.	0.8	50
58	Elastically confined martensitic transformation at the nano-scale in a multifunctional titanium alloy. Acta Materialia, 2017, 135, 330-339.	3.8	50
59	Deformation and fracture of TiN and TiAlN coatings on a steel substrate during nanoindentation. Surface and Coatings Technology, 2006, 200, 3518-3526.	2.2	48
60	Effect of tool wear evolution on chip formation during dry machining ofÂTi-6Al-4V alloy. International Journal of Machine Tools and Manufacture, 2018, 126, 13-17.	6.2	47
61	Impurity Tolerance of Unsaturated Ni-N-C Active Sites for Practical Electrochemical CO ₂ Reduction. ACS Energy Letters, 2022, 7, 920-928.	8.8	47
62	The anatomy of grain boundaries: Their structure and atomic-level solute distribution. Scripta Materialia, 2013, 69, 622-625.	2.6	46
63	Correlating Atom Probe Crystallographic Measurements with Transmission Kikuchi Diffraction Data. Microscopy and Microanalysis, 2017, 23, 279-290.	0.2	46
64	Redeposition effects in transmission electron microscope specimens of FeAl–WC composites prepared using a focused ion beam. Micron, 2003, 34, 97-107.	1.1	45
65	Detecting and extracting clusters in atom probe data: A simple, automated method using Voronoi cells. Ultramicroscopy, 2015, 150, 30-36.	0.8	44
66	The application of focused ion beam technology to the characterization of coatings. Surface and Coatings Technology, 2005, 198, 165-168.	2.2	43
67	Fabrication of dies in micro-scale for micro-sheet metal forming. Journal of Materials Processing Technology, 2006, 177, 639-643.	3.1	43
68	Tracing the coupled atomic shear and shuffle for a cubic to a hexagonal crystal transition. Scripta Materialia, 2017, 133, 70-74.	2.6	43
69	Effect of Nb Microalloying and Hot Rolling on Microstructure and Properties of Ultrathin Cast Strip Steels Produced by the CASTRIP® Process. Metallurgical and Materials Transactions A: Physical Metallurgy and Materials Science, 2011, 42, 2199-2206.	1.1	42
70	Revealing the Distribution of the Atoms within Individual Bimetallic Catalyst Nanoparticles. Angewandte Chemie - International Edition, 2014, 53, 11190-11193.	7.2	42
71	Atom probe study of impurity segregation at grain boundaries in chromia scales grown in CO2 gas. Corrosion Science, 2018, 132, 125-135.	3.0	42
72	Shaping the lens of the atom probe: Fabrication of site specific, oriented specimens and application to grain boundary analysis. Ultramicroscopy, 2011, 111, 435-439.	0.8	41

#	Article	IF	CITATIONS
73	Hydrogen trapping and desorption of dual precipitates in tempered low-carbon martensitic steel. Acta Materialia, 2020, 196, 516-527.	3.8	41
74	Phase stability of thermal barrier oxides: A comparative study of Y and Yb additions. International Journal of Materials Research, 2007, 98, 1177-1187.	0.1	40
75	Focused-ion-beam Milling: A Novel Approach to Probing the Interior of Particles Used for Inhalation Aerosols. Pharmaceutical Research, 2007, 24, 1608-1617.	1.7	40
76	A New Approach to the Determination of Concentration Profiles in Atom Probe Tomography. Microscopy and Microanalysis, 2012, 18, 359-364.	0.2	40
77	Factors that affect the properties of additively-manufactured AlSi10Mg: Porosity versus microstructure. Additive Manufacturing, 2019, 29, 100805.	1.7	40
78	Zr–Si–N films fabricated using hybrid cathodic arc and chemical vapour deposition: Structure vs. properties. Surface and Coatings Technology, 2006, 200, 4213-4219.	2.2	39
79	The influence of partitioning on the growth of intragranular α in near-β Ti alloys. Journal of Alloys and Compounds, 2015, 643, 212-222.	2.8	39
80	Transmission electron microscopy of TiN and TiAlN thin films using specimens prepared by focused ion beam milling. Surface and Coatings Technology, 2004, 183, 239-246.	2.2	38
81	Effect of coating thickness on the deformation mechanisms in PVD TiN-coated steel. Surface and Coatings Technology, 2010, 204, 1764-1773.	2.2	38
82	Significantly Raised Visibleâ€Light Photocatalytic H ₂ Evolution on a 2D/2D ReS ₂ /In ₂ ZnS ₄ van der Waals Heterostructure. Small, 2021, 17, e2100296.	5.2	38
83	Applying computational geometry techniques for advanced feature analysis in atom probe data. Ultramicroscopy, 2013, 132, 100-106.	0.8	37
84	The role of ω in the precipitation of Î \pm in near-Î 2 Ti alloys. Scripta Materialia, 2016, 117, 92-95.	2.6	37
85	Effect of niobium clustering and precipitation on strength of an NbTi-microalloyed ferritic steel. Materials Science & Engineering A: Structural Materials: Properties, Microstructure and Processing, 2014, 607, 226-235.	2.6	36
86	A study on novel AISI 304 stainless steel matrix composites reinforced with (Nb0.75,Ti0.25)C. Wear, 2018, 398-399, 220-226.	1.5	36
87	Deformation and fracture of Ti–Si–N nanocomposite films. Thin Solid Films, 2005, 479, 193-200.	0.8	35
88	Fabrication and characterization of microstructure of stainless steel matrix composites containing up to 25vol% NbC. Materials Characterization, 2016, 119, 65-74.	1.9	35
89	Effect of austenite deformation temperature on Nb clustering and precipitation in microalloyed steel. Scripta Materialia, 2014, 75, 74-77.	2.6	34
90	New frontiers in atom probe tomography: a review of research enabled by cryo and/or vacuum transfer systems. Materials Today Advances, 2020, 7, 100090.	2.5	34

#	Article	IF	CITATIONS
91	Plastic Deformation of Singleâ€Crystal Diamond Nanopillars. Advanced Materials, 2020, 32, e1906458.	11.1	34
92	Optimisation of specimen temperature and pulse fraction in atom probe microscopy experiments on a microalloyed steel. Ultramicroscopy, 2011, 111, 648-651.	0.8	33
93	The effect of pre-existing defects on the strength and deformation behavior of α-Fe nanopillars. Acta Materialia, 2013, 61, 439-452.	3.8	33
94	Linking stress-driven microstructural evolution in nanocrystalline aluminium with grain boundary doping of oxygen. Nature Communications, 2016, 7, 11225.	5.8	33
95	Transmission Electron Microscope Specimen Preparation of Metal Matrix Composites Using the Focused Ion Beam Miller. Microscopy and Microanalysis, 2000, 6, 452-462.	0.2	32
96	Crystal structures of orthorhombic, hexagonal, and cubic compounds of the Sm(x)Yb(2â^'x)TiO5 series. Journal of Solid State Chemistry, 2014, 213, 182-192.	1.4	31
97	Breaking the icosahedra in boron carbide. Proceedings of the National Academy of Sciences of the United States of America, 2016, 113, 12012-12016.	3.3	31
98	Nucleation driving force for ω-assisted formation of α and associated ω morphology in β-Ti alloys. Scripta Materialia, 2018, 155, 149-154.	2.6	31
99	Slurry erosion, sliding wear and corrosion behavior of martensitic stainless steel composites reinforced in-situ with NbC particles. Wear, 2019, 420-421, 149-162.	1.5	31
100	Site-specific specimen preparation for atom probe tomography of grain boundaries. Physica B: Condensed Matter, 2007, 394, 267-269.	1.3	30
101	Thin-film nanocomposites of diamond-like carbon and titanium oxide; Osteoblast adhesion and surface properties. Diamond and Related Materials, 2010, 19, 329-335.	1.8	30
102	Resolving the Morphology of Niobium Carbonitride Nano-Precipitates in Steel Using Atom Probe Tomography. Microscopy and Microanalysis, 2014, 20, 1100-1110.	0.2	30
103	Atom probe study of chromium oxide spinels formed during intergranular corrosion. Scripta Materialia, 2015, 99, 1-4.	2.6	30
104	Performance of graphene, carbon nanotube, and gold nanoparticle chemiresistor sensors for the detection of petroleum hydrocarbons in water. Journal of Nanoparticle Research, 2014, 16, 1.	0.8	29
105	Interpreting atom probe data from chromium oxide scales. Ultramicroscopy, 2015, 159, 354-359.	0.8	29
106	Microstructure characterisation and mechanical properties of a functionally-graded NbC/high chromium white cast iron composite. Materials Characterization, 2018, 136, 196-205.	1.9	29
107	Deposition of nanocomposite TiN-Si3N4 thin films by hybrid cathodic arc and chemical vapor process. Applied Physics A: Materials Science and Processing, 2005, 81, 151-158.	1.1	28
108	Martensitic transformation in an intergranular corrosion area of austenitic stainless steel during thermal cycling. Corrosion Science, 2014, 85, 1-6.	3.0	28

Julie Cairney

#	Article	IF	CITATIONS
109	Mapping interfacial excess in atom probe data. Ultramicroscopy, 2015, 159, 438-444.	0.8	28
110	Microstructural investigation of Ti–Si–N hard coatings. Scripta Materialia, 2010, 63, 192-195.	2.6	27
111	Effect of electrolyte storage layer on performance of PPy-PVDF-PPy microactuators. Sensors and Actuators B: Chemical, 2011, 155, 810-816.	4.0	27
112	Pushing the Limits for Microactuators Based on Electroactive Polymers. Journal of Microelectromechanical Systems, 2012, 21, 574-585.	1.7	27
113	A new systematic framework for crystallographic analysis of atom probe data. Ultramicroscopy, 2015, 154, 7-14.	0.8	27
114	Atom probe tomography analysis of the reference zircon gj-1: An interlaboratory study. Chemical Geology, 2018, 495, 27-35.	1.4	27
115	High strength heat-treatable β-titanium alloy for additive manufacturing. Materials Science & Engineering A: Structural Materials: Properties, Microstructure and Processing, 2020, 791, 139646.	2.6	27
116	Deposition of nanocomposite thin films by a hybrid cathodic arc and chemical vapour technique. Surface and Coatings Technology, 2006, 201, 4139-4144.	2.2	26
117	Cluster strengthening of Nb-microalloyed ultra-thin cast strip steels produced by the CASTRIP® process. Materials Science & Engineering A: Structural Materials: Properties, Microstructure and Processing, 2013, 568, 88-95.	2.6	26
118	Nanoscale pathways for human tooth decay – Central planar defect, organic-rich precipitate and high-angle grain boundary. Biomaterials, 2020, 235, 119748.	5.7	26
119	Characterization of TiN thin films subjected to nanoindentation using focused ion beam milling. Applied Surface Science, 2004, 237, 627-631.	3.1	25
120	The rise of computational techniques in atom probe microscopy. Current Opinion in Solid State and Materials Science, 2013, 17, 224-235.	5.6	25
121	Stabilizing the body centered cubic crystal in titanium alloys by a nano-scale concentration modulation. Journal of Alloys and Compounds, 2017, 700, 155-158.	2.8	25
122	Laser-Assisted Atom Probe Tomography of Deformed Minerals: A Zircon Case Study. Microscopy and Microanalysis, 2017, 23, 404-413.	0.2	25
123	Roles of Nd and Mn in a new creep-resistant magnesium alloy. Materials Science & Engineering A: Structural Materials: Properties, Microstructure and Processing, 2020, 779, 139152.	2.6	25
124	Preparation of transmission electron microscope specimens from FeAl and WC powders using focused-ion beam milling. Materials Characterization, 2001, 46, 297-304.	1.9	24
125	Trace element homogeneity from micron- to atomic scale: Implication for the suitability of the zircon GJ-1 as a trace element reference material. Chemical Geology, 2017, 456, 10-18.	1.4	24
126	Three dimensional imaging of deformation modes in TiN-based thin film coatings. Thin Solid Films, 2007, 515, 3190-3195.	0.8	23

#	Article	IF	CITATIONS
127	Examination of fracture surfaces using focused ion beam milling. Scripta Materialia, 2000, 42, 473-478.	2.6	22
128	Precipitation of the α-phase in an ultrafine grained beta-titanium alloy processed by severe plastic deformation. Materials Science & Engineering A: Structural Materials: Properties, Microstructure and Processing, 2014, 605, 144-150.	2.6	22
129	Threeâ€dimensional nanofabrication of polystyrene by focused ion beam. Journal of Microscopy, 2012, 248, 129-139.	0.8	21
130	The effect of clustering on the mobility of dislocations during aging in Nb-microalloyed strip cast steels: In situ heating TEM observations. Scripta Materialia, 2013, 69, 481-484.	2.6	21
131	Insight into the deformation mechanisms of $\hat{i}\pm$ -Fe at the nanoscale. Scripta Materialia, 2011, 65, 1037-1040.	2.6	20
132	Ion-irradiation resistance of the orthorhombic Ln2TiO5 (LnÂ=ÂLa, Pr, Nd, Sm, Eu, Gd, Tb and Dy) series. Journal of Nuclear Materials, 2015, 467, 683-691.	1.3	20
133	Continuous and reversible atomic rearrangement in a multifunctional titanium alloy. Materialia, 2018, 2, 1-8.	1.3	20
134	Designing Co3O4/silica catalysts and intensified ultrafiltration membrane-catalysis process for wastewater treatment. Chemical Engineering Journal, 2021, 419, 129465.	6.6	20
135	Predicting the fatigue life of an AlSi10Mg alloy manufactured via laser powder bed fusion by using data from computed tomography. Additive Manufacturing, 2020, 32, 100899.	1.7	19
136	Crystal chemistry of the orthorhombic Ln2TiO5 compounds with Ln=La, Pr, Nd, Sm, Gd, Tb and Dy. Journal of Solid State Chemistry, 2015, 227, 60-67.	1.4	18
137	Performance of an FeCrAl alloy in a high-temperature CO2 environment. Corrosion Science, 2018, 139, 267-274.	3.0	18
138	Ultrahigh-strength submicron-sized metallic glass wires. Scripta Materialia, 2014, 84-85, 27-30.	2.6	17
139	Point-by-point compositional analysis for atom probe tomography. MethodsX, 2014, 1, 12-18.	0.7	17
140	Some factors affecting EBSD pattern quality of Ga+ ion-milled face centred cubic metal surfaces. Materials Chemistry and Physics, 2007, 106, 142-148.	2.0	16
141	Overcoming challenges in the study of nitrided microalloyed steels using atom probe. Ultramicroscopy, 2012, 112, 32-38.	0.8	15
142	Elemental distributions within multiphase quaternary Pb chalcogenide thermoelectric materials determined through three-dimensional atom probe tomography. Nano Energy, 2016, 26, 157-163.	8.2	15
143	The influence of crystal structure on ion-irradiation tolerance in the Sm(x)Yb(2-x)TiO5 series. Journal of Nuclear Materials, 2016, 471, 17-24.	1.3	15
144	Precipitation of (Ti, Zr, Nb, Ta, Hf)C high entropy carbides in a steel matrix. Materialia, 2020, 9, 100540.	1.3	15

#	Article	IF	CITATIONS
145	Versatile direct-writing of dopants in a solid state host through recoil implantation. Nature Communications, 2020, 11, 5039.	5.8	15
146	The crystal structures and corresponding ion-irradiation response for the Tb(x)Yb(2â^'x)TiO5 series. Ceramics International, 2018, 44, 511-519.	2.3	15
147	New atom probe approaches to studying segregation in nanocrystalline materials. Ultramicroscopy, 2013, 132, 158-163.	0.8	14
148	A computational geometry framework for the optimisation of atom probe reconstructions. Ultramicroscopy, 2016, 169, 62-68.	0.8	14
149	Atoms on the move—finding the hydrogen. Science, 2017, 355, 1128-1129.	6.0	14
150	Flame-made amorphous solid acids with tunable acidity for the aqueous conversion of glucose to levulinic acid. Green Chemistry, 2020, 22, 688-698.	4.6	14
151	A multi-ion plasma FIB study: Determining ion implantation depths of Xe, N, O and Ar in tungsten via atom probe tomography. Ultramicroscopy, 2021, 228, 113334.	0.8	14
152	Giant room temperature compression and bending in ferroelectric oxide pillars. Nature Communications, 2022, 13, 335.	5.8	14
153	Defining the Potential of Nanoscale Reâ€Os Isotope Systematics Using Atom Probe Microscopy. Geostandards and Geoanalytical Research, 2018, 42, 279-299.	1.7	13
154	Analytical Techniques for Probing Small-Scale Layers that Preserve Information on Gas–Solid Interactions. Reviews in Mineralogy and Geochemistry, 2018, 84, 103-175.	2.2	13
155	Fracture toughness testing using photogrammetry and digital image correlation. MethodsX, 2018, 5, 1166-1177.	0.7	13
156	The ion-irradiation tolerance of the pyrochlore to fluorite Ho(x)Yb(2-x)TiO5 and Er2TiO5 compounds: A TEM comparative study using both in-situ and bulk ex-situ irradiation approaches. Journal of Nuclear Materials, 2018, 507, 316-326.	1.3	13
157	Thin film composites of nanocrystalline ZrO2 and diamond-like carbon: Synthesis, structural properties and bone cell proliferation. Acta Biomaterialia, 2010, 6, 4154-4160.	4.1	12
158	Advanced volume reconstruction and data mining methods in atom probe tomography. MRS Bulletin, 2016, 41, 46-52.	1.7	12
159	Real-time observation of stress-induced domain evolution in a [011]ÂPIN-PMN-PT relaxor ferroelectric single crystal. Acta Materialia, 2019, 175, 436-444.	3.8	12
160	Understanding the mechanical behavior of nanocrystalline Al–O thin films with complex microstructures. Acta Materialia, 2014, 77, 269-283.	3.8	11
161	Influence of Ni Solute segregation on the intrinsic growth stresses in Cu(Ni) thin films. Scripta Materialia, 2016, 113, 131-134.	2.6	11
162	A New Approach to Understand the Adsorption of Thiophene on Different Surfaces: An Atom Probe Investigation of Self-Assembled Monolayers. Langmuir, 2017, 33, 9573-9581.	1.6	11

#	Article	IF	CITATIONS
163	Thermally stable epitaxial ZrN/carrier-compensated Sc0.99Mg0.01N metal/semiconductor multilayers for thermionic energy conversion. Journal of Materials Science, 2020, 55, 1592-1602.	1.7	11
164	Understanding the role of facets and twin defects in the optical performance of GaAs nanowires for laser applications. Nanoscale Horizons, 2021, 6, 559-567.	4.1	11
165	The Hidden Pathways in Dense Energy Materials – Oxygen at Defects in Nanocrystalline Metals. Advanced Materials, 2015, 27, 6220-6224.	11.1	10
166	A Gas-Phase Reaction Cell for Modern Atom Probe Systems. Microscopy and Microanalysis, 2019, 25, 410-417.	0.2	10
167	Carbon-Coating Layers on Boron Generated High Critical Current Density in MgB2 Superconductor. ACS Applied Materials & Interfaces, 2020, 12, 8563-8572.	4.0	10
168	Micron-scale polymer–metal cantilever actuators fabricated by focused ion beam. Sensors and Actuators A: Physical, 2011, 172, 462-470.	2.0	9
169	Atom probe microscopy characterization of as quenched Zr–0.8wt% Fe and Zr–0.15wt% Cr binary alloys. Materials Letters, 2013, 91, 63-66.	1.3	9
170	Correlating spatial, temporal and chemical information in atom probe data: new insights from multiple evaporation in microalloyed steels. Philosophical Magazine Letters, 2013, 93, 299-306.	0.5	9
171	Cryo Atom Probe: Freezing atoms in place for 3D mapping. Nano Today, 2021, 37, 101107.	6.2	9
172	On the Viability of FIB Tomography for Generating 3-D Orientation Maps in Deformed and Annealed Metals. Materials Science Forum, 2007, 550, 55-64.	0.3	8
173	Effects of Si, Mn, and water vapour on the microstructure of protective scales grown on Fe–20Cr in CO ₂ gas. Materials at High Temperatures, 2018, 35, 22-29.	0.5	8
174	Interpreting Atom Probe Data from Oxide–Metal Interfaces. Microscopy and Microanalysis, 2018, 24, 342-349.	0.2	8
175	The effect of hydrogen on the early stages of oxidation of a magnesium alloy. Corrosion Science, 2020, 165, 108391.	3.0	8
176	Atom Probe Tomography of Encapsulated Hydroxyapatite Nanoparticles. Small Methods, 2021, 5, e2000692.	4.6	8
177	Laser ablation sample preparation for atom probe tomography and transmission electron microscopy. Ultramicroscopy, 2021, 220, 113161.	0.8	8
178	Effect of T6 treatment on additively-manufactured AlSi10Mg sliding against ceramic and steel. Wear, 2021, 482-483, 203961.	1.5	8
179	Integrative Atom Probe Tomography Using Scanning Transmission Electron Microscopy-Centric Atom Placement as a Step Toward Atomic-Scale Tomography. Microscopy and Microanalysis, 2021, 27, 140-148.	0.2	8
180	Simultaneous Large Optical and Piezoelectric Effects Induced by Domain Reconfiguration Related to Ferroelectric Phase Transitions. Advanced Materials, 2022, 34, e2106827.	11.1	8

#	Article	IF	CITATIONS
181	The Influence of Microscope and Specimen Parameters on the Spatial Resolution of Transmission Kikuchi Diffraction. Microscopy and Microanalysis, 2017, 23, 532-533.	0.2	7
182	Bridging metal-ion induced vertical growth of MoS2 and overall fast electron transfer in (C,P)3N4-M (Ni2+, Co2+)-MoS2 electrocatalyst for efficient hydrogen evolution reaction. Sustainable Materials and Technologies, 2020, 25, e00172.	1.7	7
183	Analysis Techniques for Atom Probe Tomography. Springer Series in Materials Science, 2012, , 213-297.	0.4	7
184	A simple approach to atom probe sample preparation by using shadow masks. Ultramicroscopy, 2016, 160, 163-167.	0.8	6
185	Additive manufacturing of a novel alpha titanium alloy from commercially pure titanium with minor addition of Mo2C. Materialia, 2018, 4, 227-236.	1.3	6
186	Nanoscale Analysis of Corrosion Products: A Review of the Application of Atom Probe and Complementary Microscopy Techniques. Jom, 2018, 70, 1744-1751.	0.9	6
187	Overcoming Challenges Associated with the Analysis of Nacre by Atom Probe Tomography. Geostandards and Geoanalytical Research, 2019, 43, 385-395.	1.7	6
188	Lateral Gating of 2D Electron Gas in Cross ectional LaAlO 3 /SrTiO 3. Advanced Electronic Materials, 2020, 6, 2000068.	2.6	6
189	Solution Epitaxy of Halide Perovskite Thin Single Crystals for Stable Transistors. ACS Applied Materials & Interfaces, 2021, 13, 37840-37848.	4.0	6
190	Specimen Preparation. Springer Series in Materials Science, 2012, , 71-110.	0.4	6
191	Challenges Associated with the Characterisation of Nanocrystalline Materials Using Atom Probe Tomography. Materials Science Forum, 2010, 654-656, 2366-2369.	0.3	5
192	Investigating Stress-Assisted Grain Growth in Nanocrystalline Materials Using in-situ Transmission Kikuchi Diffraction. Microscopy and Microanalysis, 2017, 23, 538-539.	0.2	5
193	Advanced concentration analysis of atom probe tomography data: Local proximity histograms and pseudo-2D concentration maps. Ultramicroscopy, 2018, 189, 61-64.	0.8	5
194	Novel complex ceramic oxides, Ln ₂ TiO ₅ (LnÂ=ÂLa, Sm, Gd, Tb, Dy, Ho, Er, and Yb), for polyphase nuclear wasteâ€forms. Journal of the American Ceramic Society, 2020, 103, 5536-5545.	1.9	5
195	Developing Atom Probe Tomography of Phyllosilicates in Preparation for Extraâ€Terrestrial Sample Return. Geostandards and Geoanalytical Research, 2021, 45, 427-441.	1.7	5
196	Tuning Ta coating properties through chemical and plasma etching pre-treatment of NiTi wire substrates. Surface and Coatings Technology, 2021, 418, 127214.	2.2	5
197	Grain size stability in Al-Sc alloys processed by severe plastic deformation. Scripta Materialia, 2016, 123, 105-108.	2.6	4
198	A rival to superalloys at high temperatures. Science, 2020, 370, 37-38.	6.0	4

#	Article	IF	CITATIONS
199	Improving metal-ceramic systems subjected to sliding contact by reinforcing the metallic counterpart with ceramic particles. Wear, 2020, 452-453, 203311.	1.5	4
200	Tomographic Reconstruction. Springer Series in Materials Science, 2012, , 157-209.	0.4	4
201	Tribological behaviour of fused deposition modelling printed short carbon fibre reinforced nylon composites with surface textures under dry and water lubricated conditions. Friction, 2022, 10, 2045-2058.	3.4	4
202	Focused Ion Beam Fabricated Polystyrene-Platinum Thermal Microactuator. Advanced Materials Research, 0, 254, 86-89.	0.3	3
203	High Strength and Retained Ductility Achieved in a Nitrided Strip Cast Nb-Microalloyed Steel. Metallurgical and Materials Transactions A: Physical Metallurgy and Materials Science, 2013, 44, 848-855.	1.1	3
204	Vibration Energy Harvesting Using Relaxor Ferroelectric Transduction. Procedia Engineering, 2017, 188, 432-439.	1.2	3
205	Precipitation of string-shaped morphologies consisting of aligned \hat{I}_{\pm} phase in a metastable \hat{I}^2 titanium alloy. Scientific Reports, 2018, 8, 2038.	1.6	3
206	The effect of NbC morphology on the slurry erosion performance of ferrous alloys. Wear, 2019, 434-435, 202988.	1.5	3
207	From Field Desorption Microscopy to Atom Probe Tomography. Springer Series in Materials Science, 2012, , 29-68.	0.4	3
208	Redeposition Effects in TEM Sample Preparation of Feal-Based Metal Matrix Composites using the Focused Ion Beam Miller. Microscopy and Microanalysis, 2000, 6, 514-515.	0.2	2
209	Nitriding of a Nb-Microalloyed Thin Strip Cast Steel at 525°C. Materials Science Forum, 0, 654-656, 106-109.	0.3	2
210	3D-EBSD Studies of Deformation, Recrystallization and Phase Transformations. Materials Science Forum, 0, 715-716, 41-50.	0.3	2
211	An Overview of the Effect of Nb in Strengthening Castrip [®] Steel. Materials Science Forum, 2013, 753, 559-562.	0.3	2
212	The effect orientation of features in reconstructed atom probe data on the resolution and measured composition of T1 plates in an A2198 aluminium alloy. Ultramicroscopy, 2015, 159, 368-373.	0.8	2
213	Online Microscope Simulators for Training and Outreach. Microscopy and Microanalysis, 2017, 23, 2300-2301.	0.2	2
214	Atomic coordinates and polarization map around a pair of 12a[011Â⁻] dislocation cores produced by plastic deformation in relaxor ferroelectric PIN–PMN–PT. Journal of Applied Physics, 2021, 129, .	1.1	2
215	Experimental Protocols in Atom Probe Tomography. Springer Series in Materials Science, 2012, , 121-155.	0.4	2
216	Atom Probe Microscopy and Materials Science. Springer Series in Materials Science, 2012, , 299-311.	0.4	2

#	Article	IF	CITATIONS
217	Atom probe specimen preparation methods for nanoparticles. Ultramicroscopy, 2022, 233, 113420.	0.8	2
218	Preparation of Site Specific Atom Probe Tips using Focused Ion Beam Technology. Microscopy and Microanalysis, 2006, 12, 1296-1297.	0.2	1
219	Recognizing 60 years of achievements in field emission and atomic scale microscopy. Materials Today, 2016, 19, 182-183.	8.3	1
220	Atom Probe Tomography of Human Tooth Enamel and the Accurate Identification of Magnesium and Carbon in the Mass Spectrum. Microscopy and Microanalysis, 2017, 23, 676-677.	0.2	1
221	Quantitative Determination of How Growth Conditions Affect the 3D Composition of InGaAs Nanowires. Microscopy and Microanalysis, 2019, 25, 524-531.	0.2	1
222	A Comparative Investigation Between Transmission Kikuchi Diffraction (TKD) and Precession Electron Diffraction (PED). Microscopy and Microanalysis, 2020, 26, 270-271.	0.2	1
223	Nanoporous metal tips as frameworks for analysing frozen liquids with atom probe tomography. Microscopy and Microanalysis, 2021, 27, 1512-1513.	0.2	1
224	Significantly Raised Visibleâ€Light Photocatalytic H ₂ Evolution on a 2D/2D ReS ₂ /In ₂ ZnS ₄ van der Waals Heterostructure (Small 32/2021). Small, 2021, 17, 2170168.	5.2	1
225	Field Ion Microscopy. Springer Series in Materials Science, 2012, , 9-28.	0.4	1
226	Remote Learning Facilitated by MyScope Explore. Microscopy Today, 2021, 29, 42-48.	0.2	1
227	Characterisation of an ultra-thin multilayer structure for spintronic materials. , 2010, , .		0
228	Titelbild: Revealing the Distribution of the Atoms within Individual Bimetallic Catalyst Nanoparticles (Angew. Chem. 42/2014). Angewandte Chemie, 2014, 126, 11279-11279.	1.6	0
229	Investigation into Solute Stabilizing Effects in Nanocrystalline Materials: An Atom Probe Characterization Study. Microscopy and Microanalysis, 2015, 21, 357-358.	0.2	0
230	4. Analytical Techniques for Probing Small-Scale Layers that Preserve Information on Gas–Solid Interactions. , 2018, , 103-176.		0
231	Atomic-scale Observation of Hydroxyapatite Nanoparticle. Microscopy and Microanalysis, 2019, 25, 2528-2529.	0.2	0
232	Development of (Nb0.75,Ti0.25)C-Reinforced Cast Duplex Stainless Steel Composites. Metallurgical and Materials Transactions A: Physical Metallurgy and Materials Science, 2020, 51, 2366-2376.	1.1	0
233	Inside Front Cover: Atom Probe Tomography of Encapsulated Hydroxyapatite Nanoparticles (Small) Tj ETQq1 1	0.784314 4.6	rgBT /Overloo
234	Developing cryogenic and vacuum transfer capabilities at the Australian Centre for Microscopy and Microanalysis. Microscopy and Microanalysis, 2021, 27, 982-983.	0.2	0

#	Article	IF	CITATIONS
235	Atomistic structure and three-dimensional spatial distribution of oxide clusters along voids in nitride metal/semiconductor superlattices. Physical Review Materials, 2021, 5, .	0.9	Ο
236	Experimental Protocols in Field Ion Microscopy. Springer Series in Materials Science, 2012, , 111-120.	0.4	0
237	Understanding Solid Solution Strengthening at Elevated Temperatures in a Creep-Resistant Dilute Mg-Gd-Ca Alloy. SSRN Electronic Journal, 0, , .	0.4	Ο